Lifetime prediction of hygro-thermo-mechanically loaded adhesive joints using LS-DYNA and user-defined material models

Maxim Rodschei, Gunnar Possart, Paul Steinmann, Julia Mergheim

Institute of Applied Mechanics, Friedrich-Alexander-Universität Erlangen-Nürnberg, Erlangen, Germany

1 Introduction

The growing use of adhesive bonding across multiple industries requires robust design methods to ensure both functionality and safety of bonded joints. In many applications, adhesive joints are exposed to cyclic loading, which can cause fatigue damage and eventually structural failure. Furthermore, environmental factors such as temperature and humidity strongly influence their aging behavior and consequently their service life. The aim of our research is to develop a computational approach for predicting the lifetime of adhesive bonds under combined hygro-thermo-mechanical (HTM) loading using LS-DYNA and user-defined material models (UMATs). Our work builds upon the results of two preceding projects [1],[2] and involves developing a cohesive zone material model that combines linear viscoelasticity with a continuum damage mechanics approach to capture both the time-dependent behavior and the degradation of adhesive joints. Further tasks are the calibration of model parameters against experimental data and the model validation through comparisons with measurements.
This manuscript begins by introducing the modeling framework for adhesive bonds in Sec. 2. Sec. 3 presents the parameter identification methods, followed by a numerical example in Sec. 4. Finally, Sec. 5 provides a summary and an outlook of this work.

2 Modeling of adhesive joints

2.1 Discretization of bonded joints and HTM coupling

Fig.1 illustrates an adhesive bond consisting of two adherends joined by an adhesive layer. The adhesive is modeled using cohesive elements placed between the solid elements of the adherends. The cohesive and adjacent solid elements share a conforming mesh, i.e., the nodes along the contact interfaces are merged. A uniform temperature T is prescribed across the bonded joint, serving as a parameter for both diffusion and mechanical simulations. For the hygric problem, Fick´s law

$$\frac{\partial c}{\partial t} = d(T)\nabla^2 c \tag{1}$$

is solved to simulate moisture transport within the adhesive, where c denotes the moisture concentration and $d(T)$ the isotropic, temperature-dependent diffusion coefficient. A prescribed concentration c_p is imposed on the boundary nodes of the adhesive layer (highlighted as red nodes in Fig.1).

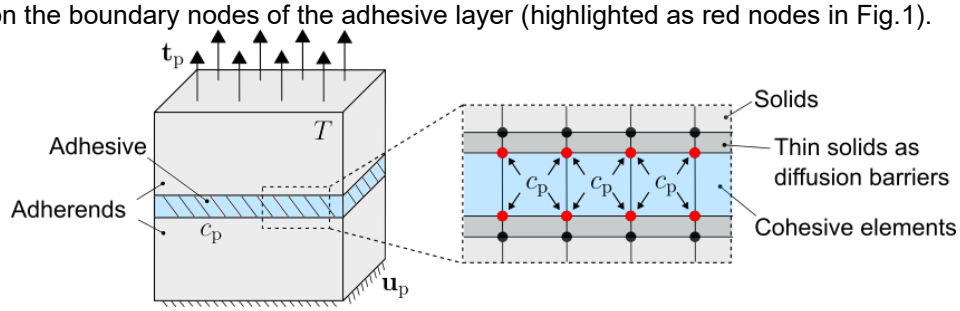

Fig.1: Adhesive bond subjected to HTM loading

To prevent moisture diffusion into the adherends, their diffusion coefficient is set to a value close to zero. In addition, the thickness of the solid elements adjacent to the cohesive zone is chosen small to reduce their numerical influence and to act as effective diffusion barriers at the common nodes. Since LS-DYNA does not provide a built-in diffusion solver, the analogy between Fick´s law and Fourier`s equation is exploited, and the thermal solver is used to simulate moisture diffusion. The LS-DYNA mechanical solver

is employed to solve the momentum balance equations with prescribed displacements $\mathbf{u}_\mathrm{p}$ and tractions $\mathbf{t}_\mathrm{p}$ on the Dirichlet and Neumann boundaries, respectively. The kinematics within the cohesive elements are described by the displacement jump vectors $[\![\mathbf{u}]\!]$, while the cohesive tractions $\mathbf{t}([\![\mathbf{u}]\!], T, c)$ define the temperature- and concentration-dependent stress state. A user-defined cohesive law is implemented via a UMAT to relate the displacement jumps to the cohesive tractions.
A one-way coupling from the hygric to the mechanical problem is assumed, and the coupled problem is solved in a staggered procedure. In each cycle, one diffusion time step is computed first. The resulting concentrations serve as input for the subsequent mechanical time steps, which are calculated until the mechanical solver reaches the diffusion time. Then, the next diffusion step is performed.

2.2 Constitutive model for adhesives

2.2.1 Linear viscoelastic law

The effective cohesive traction $\tilde{\mathbf{t}}$ in the undamaged configuration is determined via the Boltzmann Superposition Integral [3]:

$$\tilde{\mathbf{t}} = \int_0^t \boldsymbol{R}(t-s)\,\frac{d[\![\mathbf{u}]\!]}{ds}\,ds, \quad \tilde{\mathbf{t}} = \begin{bmatrix} \tilde{\mathrm{t}}_{t1} \\ \tilde{\mathrm{t}}_{t2} \\ \tilde{\mathrm{t}}_{n} \end{bmatrix}, \tag{2}$$

where t denotes the current time and s the past time. The effective traction consists of three components corresponding to the three spatial directions in the cohesive element: the tangential directions $t1$ and $t2$, and the normal direction n. The relaxation function tensor $\boldsymbol{R}(t-s)$ is given as

$$\boldsymbol{R}(t-s) = \begin{bmatrix} R_s(t-s) & 0 & 0 \\ 0 & R_s(t-s) & 0 \\ 0 & 0 & R_n(t-s) \end{bmatrix} \tag{3}$$

and comprises the shear relaxation function $R_s(t-s)$ and normal relaxation function $R_n(t-s)$. Both functions are described using Prony series

$$R_s(t-s) = k_{s\infty} + \sum_{i=1}^{M} k_{si} \exp\left(-\frac{t-s}{a_T(T)a_c(c)\tau_{si}}\right), \quad R_n(t-s) = k_{n\infty} + \sum_{i=1}^{M} k_{ni} \exp\left(-\frac{t-s}{a_T(T)a_c(c)\tau_{ni}}\right), \tag{4}$$

based on the Wiechert model [3] (see Fig.2).

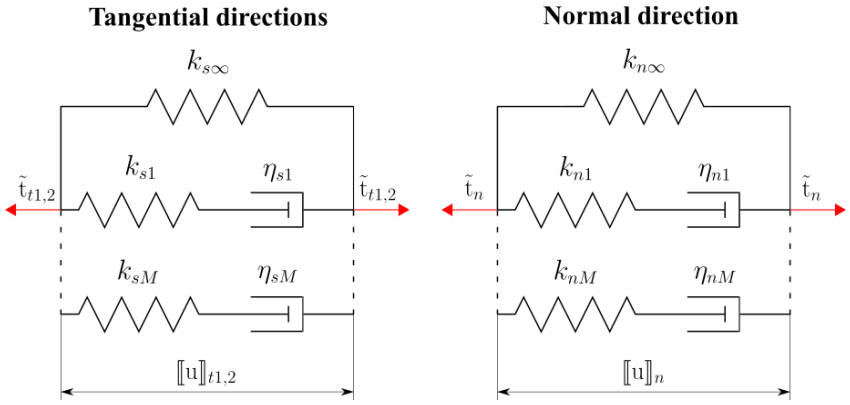

Fig.2: Wiechert model with tangential and normal contributions

Here, the stiffnesses of the equilibrium springs in tangential and normal directions are specified by the parameters $k_{s\infty}$ and $k_{n\infty}$, respectively, while k_{si} and k_{ni} represent the stiffnesses of the springs in the Maxwell elements. The relaxation times τ_{si} and τ_{ni} are given by $\tau_{si} = \eta_{si}/k_{si}$ and $\tau_{ni} = \eta_{ni}/k_{ni}$, where η_{si} and η_{ni} denote the viscosities of the dashpots.
To consider the effects of temperature and moisture on viscoelastic behavior, the time-temperature-superposition [4], [5] and time-moisture-superposition [6], [7] principles are applied. The relaxation times are multiplied by temperature shift factors $a_T(T)$ and concentration shift factors $a_c(c)$. This approach allows modeling faster or slower viscoelastic responses: increased temperature or moisture accelerates relaxation and creep, while decreased temperature or moisture slows down the material response.

2.2.2 Damage formulation

HTM loading causes a gradual degradation of adhesive bonds through both mechanical and chemical processes. To capture this effect in the constitutive model, the framework of continuum damage mechanics is employed. The effective cohesive traction is scaled by a scalar damage variable $D \in [0,1]$:

$$\mathbf{t} = [1 - D]\tilde{\mathbf{t}}, \tag{5}$$

yielding the nominal traction $\mathbf{t}$. The damage variable quantifies the local damage state in the adhesive, where $D = 0$ corresponds to the intact state, and $D = 1$ to complete failure. Its time evolution is governed by the differential equation

$$\dot{D} = \dot{D}_c + \dot{D}_f + \dot{D}_a, \tag{6}$$

which includes contributions from creep $\dot{D}_c$, fatigue $\dot{D}_f$ and chemical aging $\dot{D}_a$.
The creep contribution describes accumulation of damage under constant mechanical loading and is defined as (see also [8])

$$\dot{D}_c = \frac{1}{c_0}\left[\frac{\langle\sigma_{eq} - \sigma_{dc}\rangle}{\sigma_{ref}[1-D]}\right]^n \exp\left(p_c\left[\frac{1}{T_{ref}} - \frac{1}{T}\right]\right), \quad c_0 = 1s. \tag{7}$$

The formulation incorporates an Arrhenius-type term (see also [9],[10]) to account for the influence of temperature on material degradation. The parameter σ_{dc} denotes the creep strength, n the slope and σ_{ref} the y-intercept of the creep strength curve in a double-logarithmic stress-time diagram. The temperature factor is represented by p_c, with T_{ref} being the reference temperature.
The fatigue component is used to model damage accumulation under cyclic mechanical loading and is given by (see also [11])

$$\dot{D}_f = \left[\frac{\langle\sigma_{eq} - \sigma_{df}\rangle}{[\sigma_u - \sigma_{df}][1-D]}\right]^k \frac{\langle\dot{\sigma}_{eq}\rangle}{\sigma_u - \sigma_{df}} \exp\left(p_f\left[\frac{1}{T_{ref}} - \frac{1}{T}\right]\right). \tag{8}$$

Here, σ_{df} is the fatigue strength, k the slope and σ_u the y-intercept of the double-logarithmic fatigue strength curve, while p_f denotes the temperature factor for fatigue. Both creep and fatigue damage are driven by an equivalent stress σ_{eq}, which is defined using the components of the nominal traction and two modeling parameters b_1 and b_2:

$$\sigma_{eq} = \sqrt{\langle b_1\langle \mathrm{t}_n\rangle^2 + b_2\mathrm{t}_n + \mathrm{t}_{t1}^2 + \mathrm{t}_{t2}^2\rangle}. \tag{9}$$

The chemical aging contribution describes the moisture-induced degradation of adhesives. Following the approach in [12], it is expressed as

$$\dot{D}_a = B_a[1 - D]\left[\frac{c}{c_{\infty,ref}}\right]^l \exp\left(p_a\left[\frac{1}{T_{ref}} - \frac{1}{T}\right]\right). \tag{10}$$

Chemical degradation is characterized by the parameters $B_a, l, c_{\infty,ref}$ and p_a, while the local moisture concentration is considered as its driving force.

2.2.3 Cycle jump method

Since adhesive bonds in industrial applications typically experience millions of load cycles, simulating each individual cycle is computationally prohibitive. To address this, a cycle jump method is employed to accelerate simulations and reduce computation time, making lifetime predictions feasible even in the high-cycle fatigue regime. The core idea of this method is to identify a global trend in the state variables over a certain number of cycles and then use this information to extrapolate the variables over a longer period, effectively skipping multiple cycles. This procedure is illustrated in Fig.3 using the damage variable. Following the method suggested in [13], three consecutive damage values $D_1(t_1)$, $D_2(t_2)$ and $D_3(t_3)$, measured at the maxima of the loading function, are used to compute the damage increments $\Delta D(t_1) = D_1 - D_2$ and $\Delta D(t_2) = D_2 - D_3$. These increments are related to the constant cycle period P to obtain the slopes $s_{12} = \Delta D(t_1)/P$ and $s_{23} = \Delta D(t_2)/P$. The damage variable is then extrapolated using a Heun integrator:

$$D(t_1 + t_{jump}) = D_1 + \Delta D_{jump} = D_1 + \frac{t_{jump}}{2}\left[s_{12} + s_p(t_1 + t_{jump})\right], \tag{11}$$

where t_{jump} represents the jump size and ΔD_{jump} the damage increment to advance from D_1 to the extrapolated value $D(t_1 + t_{jump})$. The predicted slope after extrapolation $s_p(t_1 + t_{jump})$ is determined by

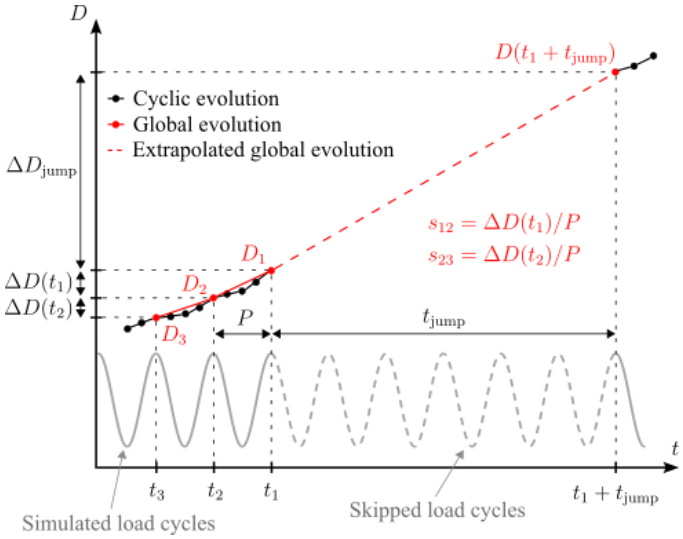

Fig.3: Damage extrapolation

$$s_p(t_1 + t_{jump}) = s_{12} + \frac{s_{12} - s_{23}}{P} t_{jump}. \tag{12}$$

Furthermore, an adaptive jump size control is implemented via a user-defined control parameter q_{jump}, which measures the relative change in the damage slope during extrapolation:

$$q_{jump} := \frac{|s_p(t_1 + t_{jump}) - s_{12}|}{|s_{12}|}. \tag{13}$$

Substituting Eq. (12) into Eq. (13) gives the jump size as a function of q_{jump}:

$$t_{jump} = \left\lfloor q_{jump} \frac{|s_{12}|}{|s_{12} - s_{23}|} \right\rfloor P, \tag{14}$$

with the floor function $\lfloor \dots \rfloor$ ensuring that the jump size is an integer multiple of P. Larger values of q_{jump} lead to a greater jump size, but potentially at the cost of an increased extrapolation error. This control parameter thus balances accuracy and computational efficiency in the cycle jump method.
In addition to damage, the viscoelastic state variables and the moisture concentrations also must be updated during jumps. An enhanced cycle jump method has been developed to account for these quantities. For brevity, this extension is not discussed here. The details are described in a separate paper, which is currently under review for publication in the International Journal of Fatigue.

3 Parameter identification

3.1 Identification of diffusion model parameters

To identify the diffusion model parameters, gravimetric analyses were performed on thin adhesive samples under different climatic conditions at the Laboratory for Materials and Joining Technology (LWF), University of Paderborn. In our model, the diffusion coefficient is expressed as a function of temperature:

$$d(T) = d_0 \exp\left(d_1 \left[\frac{1}{T_{ref}} - \frac{1}{T}\right]\right). \tag{15}$$

The measured diffusion coefficients for each sample were used to fit the parameters d_0, d_1 and T_{ref} of this function (see Fig.4, left).
In contrast, the amount of moisture that can be absorbed or released by the adhesive is assumed to depend solely on the relative humidity φ. Accordingly, a power-law formulation was used to model the mass change capacity ΔM_∞ as a function of φ:

$$\Delta M_\infty(\varphi) = M_\infty - M_{t0} = \tilde{a}\varphi^b - M_{t0}. \tag{16}$$

The parameters $\tilde{a}$, b and M_{t0} were fitted to the experimental results (see Fig.4, right). The initial moisture concentration $c_{t0} = M_{t0}/V$ and the saturation concentration $c_\infty = M_\infty/V$ of the adhesive, which serve as input parameters for the diffusion simulation, were calculated from the ratios of the initial and saturation moisture mass to the specimen volume.

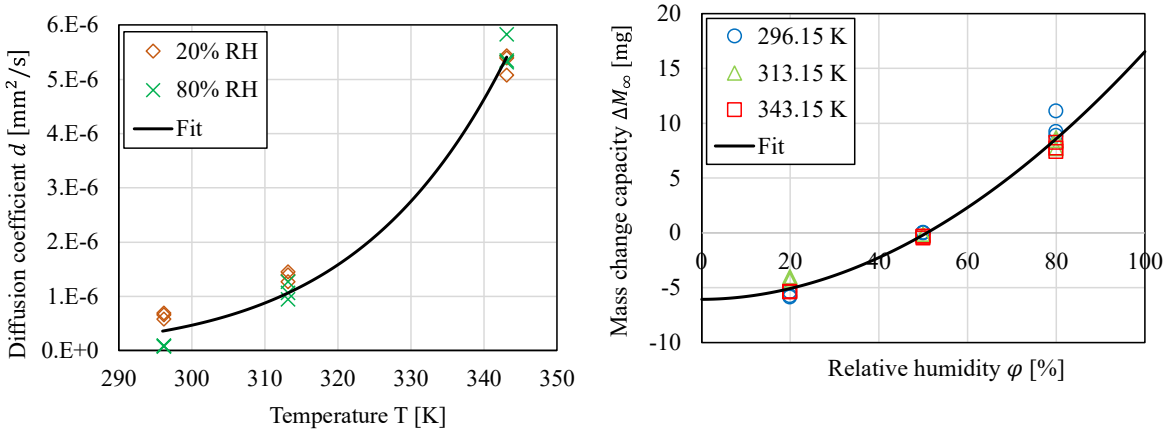

Fig.4: Function fits for diffusion coefficient (left) and mass change capacity (right)

Fig.5 compares the simulated moisture absorption and release ΔM_t of the test samples with gravimetric measurements.

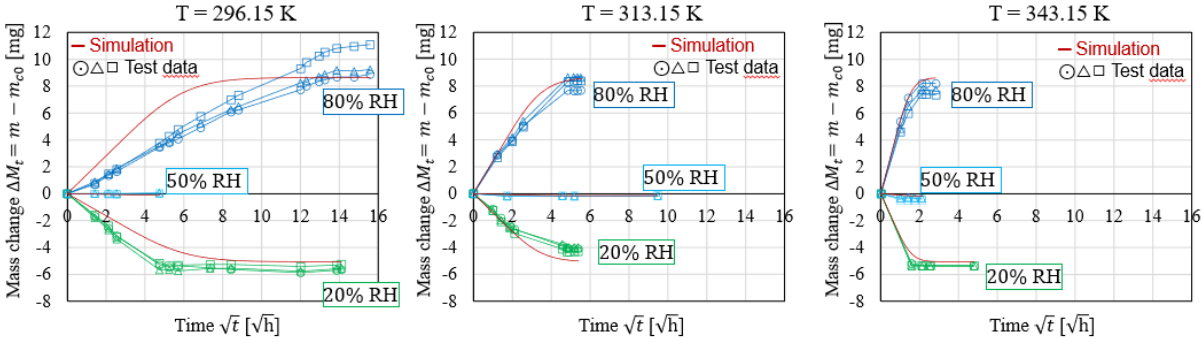

Fig.5: Comparison of simulated moisture absorption and release with gravimetric test data

The curves show good agreement, confirming the model's suitability for accurately simulating moisture diffusion in the adhesives.

3.2 Identification of viscoelastic parameters

For the identification of the viscoelastic model parameters, dynamic mechanical analyses (DMA) were conducted. Adhesive samples were subjected to temperature and cyclic frequency (ω) sweeps to determine the storage and loss moduli, $G'(T,\omega)$ and $G''(T,\omega)$. Using the time-temperature superposition principle, the moduli measured at different temperatures were shifted along the frequency axis to generate smooth, continuous master curves over a wide frequency range (see Fig.6, left).

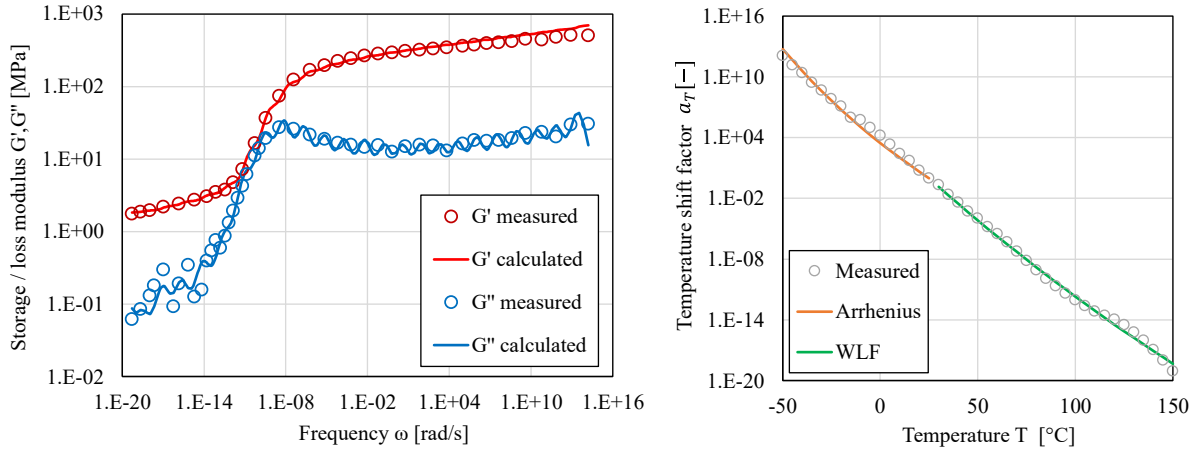

Fig.6: Fitted storage and loss modulus master curves (left) and Arrhenius/WLF models (right)

Following the algorithm presented in [14], the Prony series coefficients were obtained by fitting the measured storage and loss modulus curves through minimization of the deviations between experiment and model:

$$G'(\omega) = G_\infty + \sum_{i=1}^{M} G_i \frac{(\omega\tau_{si})^2}{1+(\omega\tau_{si})^2}, \quad G''(\omega) = \sum_{i=1}^{M} G_i \frac{\omega\tau_{si}}{1+(\omega\tau_{si})^2}. \tag{17}$$

The identified shear moduli G_∞ and G_i were subsequently transformed into the tangential stiffnesses of the cohesive zone model via $k_{s\infty} = G_\infty/d_k$ and $k_{si} = G_i/d_k$, where d_k denotes the thickness of the adhesive layer. In an analogous manner, tensile DMA tests were performed to obtain the normal stiffnesses $k_{n\infty}$ and k_{ni}, and relaxation times τ_{ni}.
The temperature shift factors are summarized in Fig.6, right. To describe the temperature dependence of the shift factor, both Arrhenius and Williams-Landel-Ferry (WLF) models [15],[16] were employed:

$$\log(a_T) = \begin{cases} \frac{-p_1[T-T_{ref}]}{p_2+T-T_{ref}} & if\ T > T_{ref} \\ p_3\left[\frac{1}{T} - \frac{1}{T_{ref}}\right] & if\ T \le T_{ref} \end{cases}, \tag{18}$$

where the parameters p_1, p_2 and p_3 were fitted to the experimental data.

3.3 Identification of damage model parameters

For the identification of the damage model parameters, creep and cyclic fatigue tests will be carried out on adhesively bonded specimens under different climatic conditions. The objective is to determine the service life of the specimens as a function of stress level, temperature, and relative humidity. The parameters of the damage model will subsequently be obtained by means of inverse identification using the optimization tool LS-OPT.

4 Numerical example

To demonstrate the lifetime model, a butt-bonded tube specimen under HTM loading was simulated (see Fig.7, left).

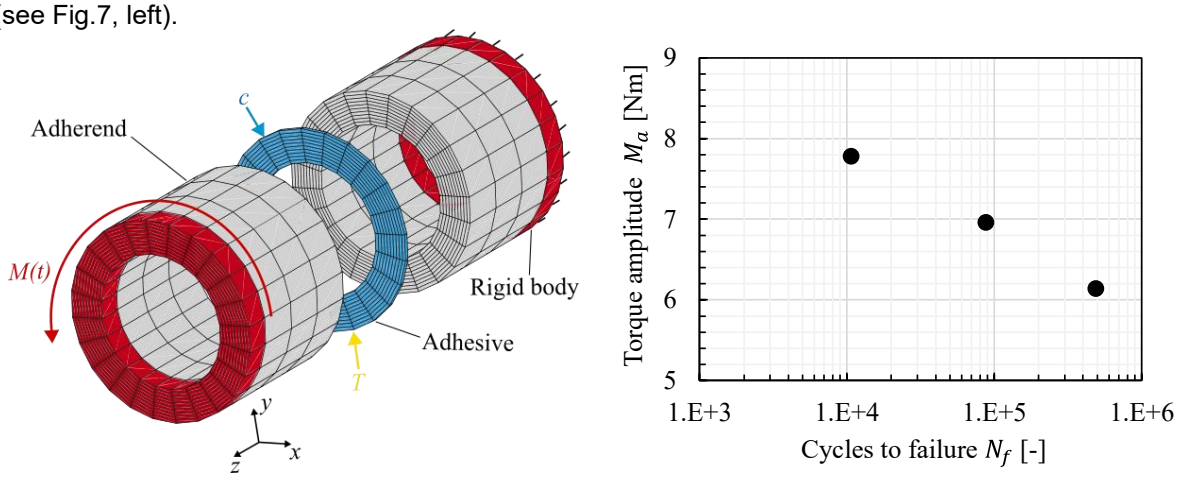

Fig.7: Butt-bonded tube specimen (left) and predicted cycles to failure (right)

The specimen consisted of two tube halves, each 12 mm in length, with an outer diameter of 15 mm and an inner diameter of 10 mm, joined by a 0.3 mm thick adhesive layer. The bond was clamped with rigid elements: one end was fixed, while a periodic torque

$$M(t) = M_m + M_a \sin(2\pi f t) \tag{19}$$

was applied at the other end. The loading frequency was set to $f = 10$ Hz, and a load ratio of $R = M_{min}/M_{max} = 0.1$ was used. For simplicity, the adhesive layer was assumed to be fully saturated, eliminating the need for explicit moisture transport simulation. Accordingly, a uniform concentration of $c = 2.05\text{E-}8$ kg/mm³ and a uniform temperature of $T = 323.15$ K were prescribed at all adhesive nodes. The joining parts were discretized using 1440 fully integrated solid elements, while the adhesive layer was represented by 240 cohesive elements. The tubes were modeled as linear elastic with a Young's modulus of $E = 210$ GPa and a Poisson's ration of $\nu = 0.3$ Since not all material parameters of the adhesive were available, data from previous projects [1],[2] were adopted. Consequently, this example was intended solely for demonstration purposes.
Three different torque amplitude levels $M_a = 7.77$ Nm, $M_a = 6.96$ Nm and $M_a = 6.14$ Nm were analyzed. The predicted numbers of cycles to failure N_f are summarized in Fig.7, right. The simulations were terminated once the damage variable in at least one cohesive element reached $D = 1$, or when the subsequent time step would have resulted in $D \ge 1$. The number of completed cycles was thereby

considered as the number of cycles to failure. As expected, increasing the load amplitude resulted in shorter lifetimes of the adhesive bond.

Fig.8 illustrates the peak equivalent stress $\sigma_{eq,max}$ and damage distribution in the adhesive layer at three representative time points during the simulation for $M_a = 7.77$ Nm. The peak equivalent stresses corresponded to the maximum stress values during the cycle, i.e., when the torque function (19) reached its maximum. Torsional loading induced the highest stresses in the outer elements of the adhesive layer, which gradually decreased toward the inner elements, as shown in the first plot at cycle number $N = 10$. At this early stage, no damage had occurred yet. At the second stage, when the cycle number reached $N = 9654$, damage had accumulated in the outer adhesive elements, with the damage variable rising to

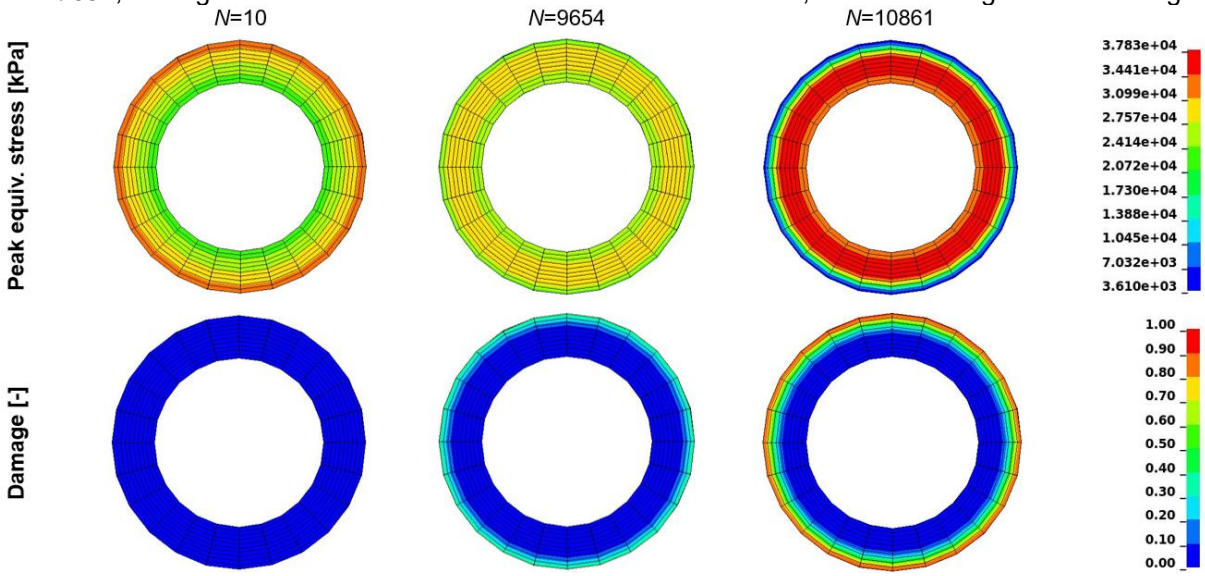

Fig.8: Equivalent stress and damage distribution in the adhesive layer at three loading stages for $M_a = 7.77$ Nm

$D = 0.3$. Consequently, the stresses in these outer elements were partially degraded and redistributed towards the inner elements. By $N = 10861$, shortly before the adhesive bond failed, damage in the outer elements was more pronounced, with the damage variable exceeding $D = 0.8$. The stresses in the outer elements were almost completely degraded and further redistributed toward the inner elements. As a result of the reduced load-bearing capacity of the adhesive layer, the overall stress levels increased, further accelerating the damage process.

The evolution of damage and its components for $M_a = 7.77$ Nm and $M_a = 6.14$ Nm is illustrated in Fig.9. At the higher loading amplitude, the mechanical damage components D_c and D_f clearly dominated, whereas the contribution of chemical aging to the overall damage was negligible.

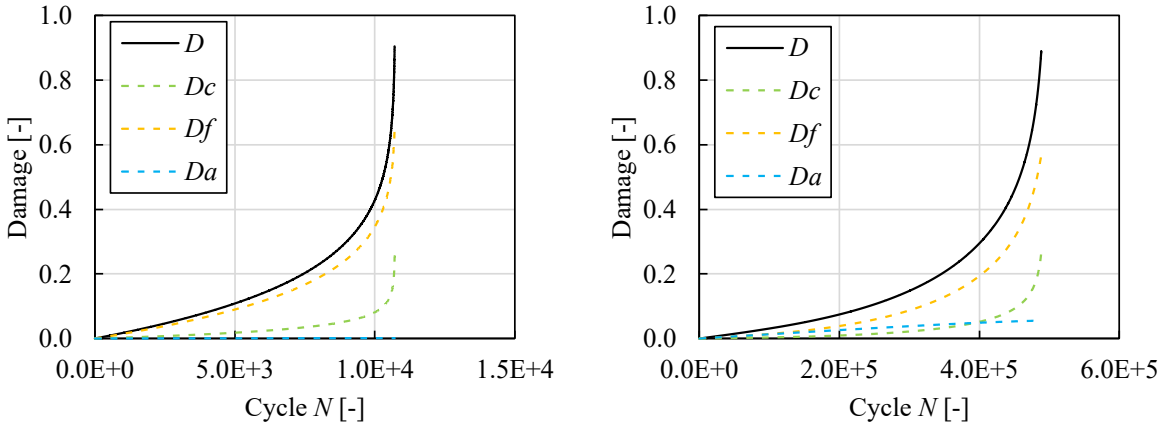

Fig.9: Damage and damage component evolutions for $M_a = 7.77$ Nm (left) and $M_a = 6.14$ Nm (right)

At the lower loading amplitude, the proportion of D_a increased relative to the total damage, as the mechanical stresses and thus the contributions of the mechanical damage components decreased. A further reduction in load amplitude would therefore increase the influence of chemical aging even more, thereby amplifying the effect of moisture on the adhesive bond's lifetime.

Finally, the effects of temperature and moisture on the lifetime of the bonded specimen were analyzed. To assess the influence of temperature, the simulations were repeated at two additional temperature values (see Fig.10, left).

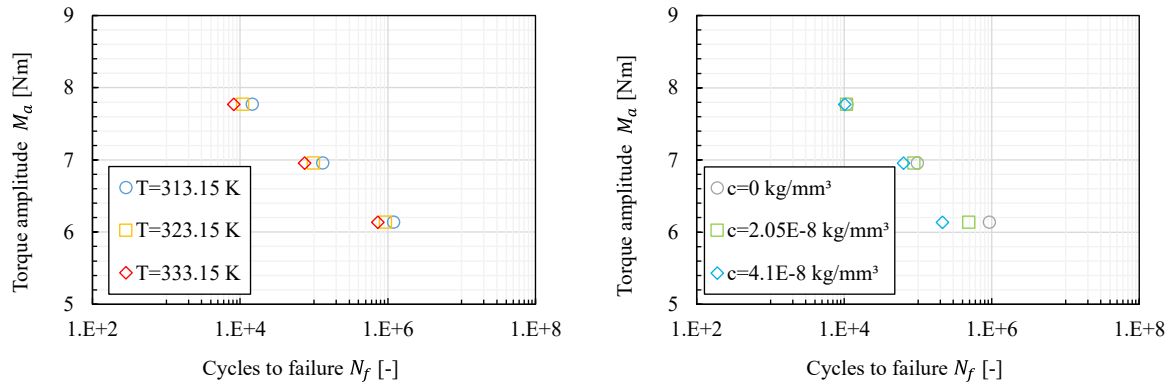

Fig.10: Effect of temperature (left) and moisture (right) on lifetime of the adhesive bond

Increasing the temperature to $T = 333.15$ K reduced the number of cycles to failure for all load amplitudes. In contrast, simulations at $T = 313.15$ K resulted in prolonged lifetimes of the adhesive bond. Similarly, the influence of moisture was studied by varying the concentration levels (see Fig.10, right). In general, higher moisture levels reduced the lifetime, with the effect being more pronounced at lower torque amplitudes, where chemical aging contributed more strongly to the overall damage.

5 Summary and outlook

In this work, a modeling framework for predicting the lifetime of adhesive bonds under HTM loading was developed. The approach involves prescribing temperature and solving one-way coupled hygro-mechanical problems using LS-DYNA together with a user-defined cohesive law implemented via the UMAT interface. A linear viscoelastic formulation combined with continuum damage mechanics was employed to capture degradation due to creep, fatigue, and moisture-induced chemical aging. Model parameters for moisture diffusion and viscoelasticity were derived from gravimetric analyses and DMA measurements. A numerical example demonstrated the plausibility of the proposed approach, although not all model parameters have been identified yet.

Ongoing work focuses on evaluating the influence of moisture on viscoelastic material behavior using DMA data at different relative humidity levels. Future steps include the identification of the remaining viscoelastic and damage model parameters through inverse parameter fitting with LS-OPT, followed by validation of the lifetime model on component-like adhesive joints, representative of coupled HTM conditions in real industrial applications.

6 Literature

[1] Çavdar, S, Meschut, G, Teutenberg, D, Matzemiller, A, Kroll, U, Brede, M, et al: "Analyse der Schwingfestigkeit geklebter Stahlverbindungen unter mehrkanaliger Belastung", FOSTA-Report P1028, Forschungsvereinigung Stahlanwendung e.V., Verlag und Vertriebsgesellschaft mbH, Düsseldorf, 2022.

[2] Sander, S, Kroll, U, Meschut, G, Matzenmiller, A: "Methodenentwicklung zur Langzeitprognose von Klebverbindungen bei kombinierter Temperatur- und Medieneinwirkung“, FOSTA-Report P1243, Forschungsvereinigung Stahlanwendung e.V., Verlag und Vertriebsgesellschaft mbH, Düsseldorf, 2022.

[3] Tschoegl, NW: "The phenomenological theory of linear viscoelastic behavior: an introduction", Springer Berlin Heidelberg, 1989.

[4] Findley, WN, Lai, JS, Onaran, K: “Creep and relaxation of nonlinear viscoelastic materials: with an introduction to linear viscoelasticity”, Dover Publications New York, 1989.

[5] Morland, LW, Lee, EH: ”Stress analysis for linear viscoelastic materials with temperature variation”, Transactions of the Society of Rheology, 4(1), 1960, 233-263.

[6] Onogi, S, Sasaguri, K, Adachi, T, Ogihara, S: “Time-humidity superposition in some crystalline polymers”, Journal of Polymer Science, 58(166), 1962, 1-17.

[7] Maksimov, RD, Mochalov, VP, Urzhumtsev, YS: “Time-moisture superposition”, Polymer Mechanics, 8(5), 1972, 685-689.

[8] Kachanov, LM: “Rupture time under creep conditions”, International Journal of Fracture, 97, 1999, 11-18.

[9] Perrin, IJ, Hayhurst, DR: “Creep constitutive equations for a 0.5Cr-0.5Mo-0.25V ferritic steel in the temperature range 600-675°C”, Journal of Strain Analysis for Engineering Design, 31(4), 1996, 299-314.
[10] L’vov, GI, Lysenko, SV, Gorash, EN: “Creep and creep-rupture strength of gas turbine components in view of nonuniform temperature distribution”, Strength of Materials, 40(5), 2008, 525-530.
[11] Lemaitre, J: “Damage modelling for prediction of plastic or creep fatigue failure in structures”, Transactions of the 5th International Conference on Structural Mechanics in Reactor Technology (SMiRT 5), Berlin, 1979.
[12] Johlitz, M, Lion, A: “Chemo-thermomechanical ageing of elastomers based on multiphase continuum mechanics”, Continuum Mechanics and Thermodynamics, 25(5), 2013, 605-624.
[13] Cojocaru, D, Karlsson, AM: “A simple numeric method of cycle jumps cyclically loaded structures”, International Journal of Fatigue, 28, 2006, 1677-1689.
[14] Baumgaertel, M, Winter, HM: “Determination of discrete relaxation and retardation time spectra from dynamic mechanical data”, Rheologica Acta, 28, 1989, 511-519.
[15] Williams, ML, Landel, RF, Ferry, JD: “The temperature dependence of relaxation mechanisms in amorphous polymers and other glass-forming liquids”, Journal of the American Chemical Society, 77(14), 1955, 3701-3707.
[16] Ferry, JD: “Viscoelastic properties of polymers”, John Wiley & Sons, Inc New York, 1980.